Magnetic structures and excitations in a multiferroic Y-type hexaferrite BaSrCo_{2}Fe_{11}AlO_{22}

Taro Nakajima, Yusuke Tokunaga, Masaaki Matsuda, Sachith Dissanayake, Jaime Fernandez-Baca, Kazuhisa Kakurai, Yasujiro Taguchi, Yoshinori Tokura, and Taka-hisa Arima

Phys. Rev. B **94**, 195154 — Published 30 November 2016

DOI: 10.1103/PhysRevB.94.195154

Magnetic structures and excitations in a multiferroic Y-type hexaferrite $BaSrCo_2Fe_{11}AlO_{22}$

Taro Nakajima,[1,*] Yusuke Tokunaga,[1,2] Masaaki Matsuda,[3] Sachith Dissanayake,[3] Jaime Fernandez-Baca,[3] Kazuhisa Kakurai,[1,4,†] Yasujiro Taguchi,[1] Yoshinori Tokura,[1,5] and Taka-hisa Arima[1,2]

[1]*RIKEN Center for Emergent Matter Science (CEMS), Saitama 351-0198, Japan.*

[2]*Department of Advanced Materials Science, University of Tokyo, Kashiwa 277-8561, Japan*

[3]*Quantum Condensed Matter Division, Oak Ridge National Laboratory, Oak Ridge, Tennessee 37831, USA*

[4]*Quantum Beam Science Center, Japan Atomic Energy Agency, Tokai, Ibaraki 319-1195, Japan*

[5]*Department of Applied Physics and Quantum Phase Electronics Center (QPEC), University of Tokyo, Tokyo 113-8656, Japan*

Abstract

We have investigated magnetic orders and excitations in a Y-type hexaferrite $BaSrCo_2Fe_{11}AlO_{22}$ (BSCoFAO), which was reported to exhibit spin-driven ferroelectricity at room temperature [Hirose *et al.*, Appl. Phys. Lett. **104**, 022907 (2014)]. By means of magnetization, electric polarization and neutron diffraction measurements using single-crystal samples, we establish H-T magnetic phase diagram for magnetic field perpendicular to the c axis ($H_{\perp c}$). This system exhibits an alternating longitudinal conical (ALC) magnetic structure in the ground state, and it turns into a non-coplanar commensurate magnetic order with spin-driven ferroelectricity under $H_{\perp c}$. The field-induced ferroelectric phase remains as a metastable state after removing magnetic field below ~ 250 K. This metastability is the key to understanding of magnetic-field-reversal of the spin-driven electric polarization in this system. Inelastic polarized neutron scattering measurements in the ALC phase reveal a magnetic excitation at around 7.5 meV, which is attributed to spin components oscillating in a plane perpendicular to the cone axis. This phason-like excitation is expected to be electric-field-active magnon, i.e., electromagnon excitation, in terms of the magnetostriction mechanism.

PACS numbers: 75.25.-j, 78.70.Nx, 75.85.+t

I. INTRODUCTION

Magneto-electric (ME) multiferroics, which simultaneously exhibit ferroelectricity and magnetic order, have been extensively investigated since the discovery of ferroelectricity in $TbMnO_3$ with a cycloidal magnetic order[1,2]. The coexistence of the two orders often enables mutual control of magnetic and dielectric properties by applying electric and magnetic fields, respectively. Thus, the ME multiferroics are expected to be applicable for new electronic devices. Among a variety of ME multiferroics, hexaferrites are supposed to be the most promising materials for the device application, because they exhibit ferroelectricity associated with noncollinear magnetic orders in relatively low magnetic field and high temperature regions[3–13]. In the present study, we focus on a Y-type hexaferrite $BaSrCo_2Fe_{11}AlO_{22}$ (BSCoFAO). This compound was reported to exhibit spin-driven ferroelectricity and electric-field induced magnetization switching at room temperature[10]. However, the magnetic orders of BSCoFAO were not investigated in detail, partly because polycrystalline samples were used in the previous studies[10,14]. In the present study, we grow single crystals of BSCoFAO by means of a laser floating zone technique, and perform magnetization, electric polarization and neutron diffraction measurements.

The multiferroic hexaferrites have also attracted attention in terms of dynamical spin-polarization coupling[15–17]. A previous THz spectroscopy study by Kida *et al.* has revealed that another Y-type hexaferrite $Ba_2Mg_2Fe_{12}O_{22}$ (BMFO) exhibits electric-field-active magnetic excitation, which is referred to as electromagnon[15,16]. Nakajima *et al.* have recently performed inelastic polarized neutron scattering (IPNS) measurements on BMFO[17], confirming that the excitation is indeed of magnetic origin and that the magnetic excitation leads to oscillating electric polarization along the c axis via the mangetostriction mechanism. In the present study, we performed IPNS measurements on BSCoFAO to explore magnon and possible electromagnon excitations in this system.

Figure 1(a) shows the crystal structure of Y-type hexaferrites, which belongs to the space group of $R\bar{3}m$. In this paper, we employ a conventional hexagonal basis $(\boldsymbol{a}, \boldsymbol{b}, \boldsymbol{c})$ instead of the primitive rhombohedral basis $(\boldsymbol{a}_R, \boldsymbol{b}_R, \boldsymbol{c}_R)$ shown in Fig. 1(a). For BSCoFAO, the lattice constants are $a = b = 5.84$ Å, and $c = 43.33$ Å. Because there are many magnetic ions in the large unit cell, it is quite difficult to determine realistic magnetic structures in this system. Thus, we employ a block approximation used in the previous studies; specifically, the system

is divided into two kinds of ferrimagnetically-ordered blocks, which are alternately stacked along the c axis[18,19]. These blocks are referred to as 'L block' and 'S block', which have larger and smaller net magnetic moments, respectively[5,20], and the net moments are treated as classical spins. In this paper, we refer to the magnetic moment in ith L (S) block as S_i^L (S_i^S).

On the basis of the block approximation, we depict schematic magnetic structures reported in the previous studies on the Y-type hexaferrites[4,12,18–20] in Figs. 1(b)-1(e). All the magnetic structures have magnetic modulation wave vectors described as $(0, 0, q)$. This is because there are strong ferromagnetic exchange interactions perpendicular to the c axis. In addition, effective exchange interactions between S_i^L and S_i^S are dependent on averaged ionic radii of intervening Ba/Sr sites, which affect Fe-O-Fe bonding angle near the boundary of the two magnetic blocks[3,11]. This leads to long-period magnetic modulations along the c axis. For zero-field states, three magnetic structures were reported: proper-screw, longitudinal conical (LC), and alternating longitudinal conical (ALC) structures shown in Figs. 1(b), 1(c) and 1(d), respectively. In the proper-screw structure, which appears, for example, in $(Ba_{1-x}Sr_x)_2Zn_2Fe_{12}O_{22}$ (BSZFO) as the ground state[21], the magnetic moments are strongly confined in a plane perpendicular to the c axis. This in-plane anisotropy largely depends on chemical compositions. For instance, BMFO has weaker anisotropy, and exhibits the LC structure, which has the net magnetization along the c axis as well as the proper-screw component on the ab plane. The uniform magnetization component is susceptible to external magnetic fields, and thus the LC structure is easily canted by applying a relatively low magnetic field inclined from the c axis. This canted conical magnetic structure can induce electric polarization (P) in terms of the spin-current mechanism[22–24]. In fact, Ishiwata *et al.* demonstrated that BMFO exhibits spin-driven electric polarization under a canted magnetic field as low as 30 mT, and that the direction and magnitude of P can be controlled by rotating the magnetic field[5]. The c-axis components of the magnetic moments were also observed to emerge in Al-doped BSZFO[12]. While the c components of the neighboring L blocks are ferromagnetically aligned in the LC phase of BMFO, they are antiferromagnetically aligned in Al-doped BSZFO in a certain temperature and Al-concentration range; this leads to the ALC structure. Note that in the ALC structure, S_i^S is supposed to lie in the ab plane[12], because if the c-axis components of S_i^L and S_i^S were arranged in a $\uparrow\uparrow\downarrow\downarrow$ sequence along the c axis, it would lead to spontaneous electric polarization along the c axis, which has not been

reported to this date.

Under a relatively strong magnetic field ($0.1 \sim 1$ T) applied perpendicular to the c axis, a non-coplanar ferrimagnetic order with a commensurate wave vector of $(0, 0, 3/2)$ was observed in a number of Y-type hexaferrites, such as BMFO[20], (Al-doped) BSZFO[21,25], and $Ba_{0.3}Sr_{1.7}Co_2Fe_{12}O_{22}$[26]. In accordance with the previous study on BMFO by Ishiwata *et al.*[20], we refer to this field-induced phase as FE3 phase. As shown in Fig. 1(e), the FE3 phase has a double-fan structure; S_i^L and S_i^S are staggered in the ab plane and a plane parallel to both the c axis and field direction, respectively. They can be decomposed into staggered collinear and cycloidal components parallel and perpendicular to the magnetic field, respectively, as shown in Fig. 1(e); the latter accounts for electric polarization normal to both the field direction and the c axis in terms of the spin-current model. In fact, spontaneous electric polarization was observed in the FE3 phase of the hexaferrites mentioned above.

Keeping these various magnetic structures in mind, we investigate temperature and magnetic field dependence of the magnetic orders in BSCoFAO mainly for magnetic fields applied perpendicular to the c axis.

II. EXPERIMENTS

Single crystals of $BaSrCo_2Fe_{11}AlO_{22}$ of nominal composition were grown by the traveling solvent floating zone method under 10 atm of pure oxygen with use of the laser floating zone furnace (SC1-LD200x5, Canon Machinery Inc.). The floating zone furnace used in this study was similar to that reported by Ito *et al.*[27], but equipped with five laser diodes. The maximum power of each laser diode was 200 W. Sintered polycrystalline rods of nominal composition were used as both feed and seed rods in the first growth, while the grown single crystal was used as a seed rod for the next growth. Temperature of the molten zone was monitored by a radiation thermometer during the growth. The typical growth rate was 1-2 mm/h. Because the annealing in the high-pressure oxygen atmosphere is reported to be effective to reduce the electric conductivity which is harmful for electric polarization measurements, the grown crystals were subsequently annealed under 10 atm O_2 at 1100 °C for 10 hours as reported in Ref. 10.

We performed magnetization, electric polarization and neutron scattering experiments using the single-crystal samples of BSCoFAO. Temperature and magnetic field dependence of

magnetization were measured using the Magnetic Property Measurement System (Quantum Design, Inc.). For the electric polarization measurements, the sample was cut into a thin-plate shape with the surface area of 3.0 mm^2 and thickness of 0.15 mm. The surfaces, on which silver-paste electrodes were formed to measure electric polarization, were normal to the [210] direction of the crystal. The sample was loaded into the Physical Property Measurement System (Quantum Design, Inc.). After appropriate electric-field and magnetic-field cooling procedures (see Sec. III C for details), we measured displacement current with varying magnetic field using an electrometer (Keithley 6517A), and obtained magnetic field variations of P by integrating the current with respect to time.

Neutron diffraction measurements were carried out at the wide angle neutron diffractometer, WAND, in the high flux isotope reactor (HFIR) of Oak Ridge national laboratory (ORNL). We used a single crystal of BSCoFAO with a cylindrical shape whose diameter and length are 2.5 and 6.1 mm, respectively. We measured temperature dependence of diffraction profiles in zero magnetic field and in a temperature range from 4 to 400 K using a high-temperature displex, and also measured magnetic field dependence of the diffraction profiles below room temperature using a vertical-field cryomagnet with a maximum field of 5 T. In both measurements, the $(h, 0, l)$ plane was selected as the scattering plane. In the in-field measurement, the direction of the magnetic field was parallel to the [010] axis of the crystal. An incident neutron beam with a wavelength of 1.5 Å was obtained by a Ge (113) monochromator.

We also performed polarized elastic and inelastic neutron scattering measurements at the triple-axis neutron spectrometer PTAX installed in the HFIR of ORNL. We used three large crystals of BSCoFAO (total mass of 1.8 g), which were carefully co-aligned in a sample holder by using the high-energy x-ray transmission Laue camera installed at Institute of Solid State Physics, the University of Tokyo, Japan. The sample holder was set in a ^{4}He closed-cycle refrigerator. An incident polarized neutron beam was obtained by a Heusler (111) monochromator. The horizontal collimation was 48′-80′-80′-open. The direction of the neutron spin polarization was controlled by a Helmholtz coil surrounding the refrigerator and a spin flipper placed between the monochromator and the sample. We employed a pyrolytic graphite (002) and a Heusler (111) analyzers to efficiently survey dispersion relations of the magnetic excitations without polarization analysis, and to perform the polarization analysis for the scattered neutrons, respectively. The flipping ratio of the polarized neutron beam was

~ 5.8[28]. The spectrometer operated in the fixed-E_f mode with E_f (the energy of scattered neutrons) of 13.5 meV. The energy resolution at the elastic condition was 1.2 meV.

III. RESULTS AND DISCUSSIONS

A. Magnetic orders in zero field

Figure 2(a) shows temperature dependence of magnetization measured under magnetic field of 100 Oe parallel and perpendicular to the c axis ($H_{\parallel c}$ and $H_{\perp c}$). We found a small cusp anomaly in magnetization under $H_{\parallel c}$ at around 360 K (T_1), below which magnetization under $H_{\perp c}$ exhibits a thermal hysteresis. To investigate the magnetic phase transition at T_1 in more detail, we measured neutron diffraction patterns with decreasing temperature from 400 K in zero field. Figure 3 shows temperature dependence of diffraction profile along the $(1, 0, l)$ line. Because we employed the hexagonal basis for the rhombohedral crystal structure, nuclear reflections should be observed at the reciprocal lattice points $\tau_{hkl} = (h, k, l)$ which satisfy the condition of $-h+k+l = 3n$ where n is an integer. However, we also observed (relatively weak) nuclear reflections at $(1, 0, 2)$ and $(1, 0, 5)$, which violate the above condition. This indicates that this crystal contains another crystallographic domain whose a and b axes are rotated by 60 degrees about the c axis. By comparing the observed intensities of the nuclear reflections with calculations, volume fraction of the minor crystallographic domain is estimated to be $\sim 9\%$.

Above T_1, we observed incommensurate magnetic reflections with a wave vector of $(0, 0, q_{\rm IC})$, where $q_{\rm IC} = 0.6 \sim 0.75$, as shown in Fig. 3, suggesting that the magnetic structure above T_1 is the incommensurate screw-type structure shown in Fig. 1(b). We note that the incommensurate reflections were rather broad as compared to the nuclear reflections. This is probably due to distribution of the magnetic periodicity, which is supposed to be sensitive to local Co and Al concentrations. Below T_1, commensurate reflections with a wave vector of $(0, 0, 3/2)$ were observed in addition to the incommensurate reflections, as shown in Fig. 3. These commensurate reflections were not observed in the $(0, 0, l)$ line, and therefore should be attributed to the c-axis components of the magnetic moments. This suggests that the magnetic structure below T_1 is the ALC structure, which has the alternatingly-stacked c-axis component as well as the screw-type component on the ab-plane (Fig. 1(d)). Figures 2(b)

and 2(c) show temperature dependences of the integrated intensities of the commensurate and incommensurate reflections and $q_{\rm IC}$, respectively. We found that the integrated intensity of the incommensurate reflection slightly decreases when passing through the transition at T_1 on cooling. This can be interpreted that the magnetic moments, which were confined in the ab plane in the proper-screw phase, are gradually inclined toward the c axis, so that the amplitude of the screw-type magnetic modulation on the ab plane is slightly reduced just below T_1.

We also performed polarized neutron diffraction (PND) measurements at 5.2 K in zero magnetic field, in order to verify the ALC structure. Here, we introduce a Cartesian coordinate as shown in Fig. 4(a); the x, y, and z axes are parallel to the [010], [210] ($\parallel a^*$), and [001] ($\parallel c^*$) directions, respectively. Neutron spin polarization p_N was set to be parallel to the x axis (perpendicular to the scattering plane). Figures 4(b) and 4(c) show the PND profiles along $(0,0,l)$ and $(1,0,l)$ lines, respectively. Red and blue data points represent intensities measured in spin-flip (SF) and non-spin-flip (NSF) channels, respectively. We obtained the final polarization of the neutrons, P_f, which is defined as below:

$$P_f = \frac{I_{NSF} - I_{SF}}{I_{NSF} + I_{SF}}, \tag{1}$$

where $I_{NSF/SF}$ is the peak intensity of a magnetic or nuclear reflection measured in the NSF/SF channel. Figures 4(d) and 4(e) show l dependence of P_f normalized to the instrumental beam polarization P_0, along the $(0,0,l)$ and $(1,0,l)$ lines, respectively. For nuclear reflections, P_f/P_0 should be 1, because the nuclear scattering process does not affect the spin polarization of neutrons. For magnetic scattering, whose intensity is proportional to square of Fourier transformed magnetic moments projected on a plane perpendicular to the scattering vector $\boldsymbol{\kappa}(=\boldsymbol{k}_i-\boldsymbol{k}_f)$, the NSF and SF scatterings arise from the magnetic moments parallel and perpendicular to p_N, respectively. Accordingly, P_f/P_0 is described as follows:

$$\frac{P_f}{P_0} = \frac{|M^x(q)|^2 - (|M^y(q)|^2\cos^2\Theta + |M^z(q)|^2\sin^2\Theta)}{|M^x(q)|^2 + |M^y(q)|^2\cos^2\Theta + |M^z(q)|^2\sin^2\Theta}, \tag{2}$$

where $M^\alpha(q)$ ($\alpha = x, y, z$) is Fourier-transformed α-axis component of the magnetic moments with a wave vector q. Θ is an angle between the c (z) axis and $\boldsymbol{\kappa}$. Bold lines in Figs. 4(d) and 4(e) show calculated l dependence of P_f/P_0 for the ALC structure. Specifically, the incommensurate component has $M^x(q)$ and $M^y(q)$, whose amplitudes are equal to each other. Thus, on the $(0,0,l)$ and $(1,0,l)$ lines, P_f/P_0 is calculated to be 0 and $(1-\cos^2\Theta)/(1+$

$\cos^2\Theta$), respectively. The commensurate component has only the $M^z(q)$ component, and therefore P_f/P_0 is -1 for the $(1,0,l)$ line. As shown in Figs. 4(d) and 4(e), the calculated and observed values of P_f/P_0 are in good agreement, confirming that the magnetic structure at the ground state is ALC structure.

B. Magnetic-field-induced phase transitions

We measured magnetization curves under $H_{\parallel c}$ and $H_{\perp c}$ at various temperatures from 5 to 400 K. Typical M-H curves at 400, 300, and 150 K are shown in Figs. 5(a), 5(b), and 5(c), respectively. We found that the M-$H_{\parallel c}$ curves show double hysteresis loops below T_1 ($\sim$ 360 K). For instance, at 300 K, the magnetization shows small jumps at around $\pm$0.5 T (Fig. 5(b)), which are not found in the M-$H_{\parallel c}$ curve at 400 K (Fig. 5(a)). These anomalies imply a field-induced phase transition from the ALC structure to the LC structure below T_1.

For the M-$H_{\perp c}$ curves, we found significant difference in hysteresis in a low-field region between 300 and 150 K. At 300 K, the M-$H_{\perp c}$ curve measured after zero field cooling (ZFC) coincides with that measured after sweeping $H_{\perp c}$ (see the inset of Fig. 5(b)), indicating that the magnetic-field induced phase transitions are reversible at 300 K. By contrast, at 150 K, we observed a jump of magnetization at 0.1 T on the $H_{\perp c}$-increasing process after ZFC. However, this anomaly was not observed in the subsequent magnetic field sweeps, indicating that the $H_{\perp c}$-induced phase transition was irreversible at 150 K (see inset of Fig. 5(c)).

To investigate the $H_{\perp c}$-induced phase transition in more detail, we performed neutron diffraction measurements under $H_{\perp c}$ using the WAND instrument. Figures 6(b) and 6(c) show $H_{\perp c}$ dependence of the integrated intensities of magnetic and nuclear reflections on the $(0,0,l)$ and $(1,0,l)$ lines at 289 K, respectively. At the initial state after ZFC, the system is in the ALC state as revealed in Sec. III A, therefore we observed the incommensurate magnetic reflections on both lines and the commensurate magnetic reflection only on the $(1,0,l)$ line. By applying $H_{\perp c}$ of up to 0.2 T, the system undergoes the field-induced magnetic phase transition, as manifested by the jump in the magnetization shown in Fig. 6(a). We found that the incommensurate reflections disappeared at around 0.1 T, and that the commensurate magnetic reflections emerged on the $(0,0,l)$ line in addition to that on the $(1,0,l)$ line. This diffraction pattern is the same as that of the double-fan structure observed

in other multiferroic Y-type hexaferrites[12,20]. We thus conclude that BSCoFAO exhibits the FE3 (double-fan) phase under $H_{\perp c}$. When the magnetic field was removed, the incommensurate magnetic reflections were retrieved, and the commensurate magnetic reflections on the $(0, 0, l)$ line disappeared. This indicates that the system is back to the ALC state.

Subsequently, we measured $H_{\perp c}$ dependence of the diffraction profiles at 150 K. Similarly to the measurements at 300 K, the phase transition from the ALC phase to the FE3 phase was observed on a $H_{\perp c}$-increasing scan after ZFC. However, when the magnetic field was removed, the incommensurate magnetic reflections were not retrieved, and instead, the commensurate reflections remained on both the $(0, 0, l)$ and $(1, 0, l)$ lines, as shown in Figs. 6(e) and 6(f), revealing that the field-induced FE3 state persists as a metastable state in zero field. This metastable FE3 state was also reported in other hexaferrites[13,26].

We also found that the intensities of 009 and 104 reflections show remarkable field dependence. This is because these reflections contain magnetic scattering signals arising from the ferromagnetic component of the magnetic moments projected on the plane perpendicular to κ, as well as the nuclear scattering. In fact, the field dependence of the intensities nearly coincide with the M-$H_{\perp c}$ curves at both 300 and 150 K, as shown in Figs. 6(a)-6(f).

We also note that the integrated intensity of a commensurate reflection on the $(1, 0, l)$ line shows non monotonous field dependence on the field increasing scans at 150 and 300 K; it shows a maximum between the ALC and FE3 phase, as shown in Figs. 6(c) and 6(c). Interestingly, M-$H_{\perp}$ curves also show inflections on the $H_{\perp c}$-increasing processes, as indicated by doubled arrows in Figs. 6(a) and 6(d). These anomalies may be indicative of the existence of an intermediate state similar to that observed in other hexaferrite systems[20,29].

In Figs. 7(a) and 7(b), we show $H_{\perp c}$-T magnetic phase diagrams for $H_{\perp}$-increasing and decreasing processes, respectively. The phase boundaries were determined from the anomalies in M-$H_{\perp c}$ curves, and each magnetic phase was identified from the results of the neutron diffraction measurements. As revealed in Sec. III A, the true ground state is the ALC state, which appears below T_1 in ZFC, as shown in Fig. 7(a). However, once the FE3 phase is induced by applying $H_{\perp c}$, it remains as a metastable state after removing $H_{\perp c}$. The zero-field FE3 phase persists up to about 250 K, as shown in Fig. 7(b).

C. Spin-driven ferroelectricity

In the previous studies on multiferroic hexaferrites[5,12,13,20,26], the FE3 phase was reported to have spin-driven electric polarization perpendicular to both the magnetic field and c axis. Thus, we performed electric polarization measurements under applied magnetic field. Figure 8(a) shows a typical P-H curve at 150 K, which was measured by the following procedure: we applied magnetic field of 5 T, where the system is supposed to be in the field-induced collinear ferrimagnetic phase, and then reduced the magnetic field to 0.3 T with applied electric field of 1.67 MV/m. By passing through the phase boundary between the collinear ferrimagnetic phase and the FE3 phase with the electric field, a macroscopic electric polarization was induced. Finally, we removed the applied electric field at 0.3 T, and then measured displacement current with sweeping magnetic field from 0.3 T to $\pm$ 5 T. We confirmed the existence of spontaneous electric polarization in the FE3 phase, and also found that the polarity of P was reversed when the magnetization was reversed, as shown in Fig. 8(a) and its inset. As mentioned in Sec. III B, the FE3 phase remains as a metastable state on the $H_{\perp c}$-decreasing process. Thus, the magnetic-field reversal of P is supposed to be achieved by rotating the double-fan structure by 180 degrees about the c axis, which should be accompanied by a flip of a vector spin chirality $S_i \times S_j$ (Fig. 8(b)). This scenario also implies that the ferromagnetic component of the magnetic structure is always perpendicular to the c axis during the rotation. This is also consistent with the fact that the integrated intensity of the 009 reflection remains constant down to zero field, as shown in Fig. 6(e).

We also measured the displacement current with sweeping magnetic field between +0.3 and −0.3 T, at 200, 250 and 300 K. We successfully observed current pulses resulting from the reversal of P at 200 K and 250 K, as shown in Figs. 8(c) and 8(d), respectively. However, the displacement current was not discernible at 300 K, as shown in Fig. 8(e). One possible reason is occurrence of large leakage current; the resistivity of the sample is reduced with increasing temperature, leading to large background current. Another reason is that the system is back to the ALC state in zero magnetic field at 300 K. Because the phase transition from the FE3 phase to the ALC phase is the first-order phase transition, the ferroic arrangement of the vector spin chirality would disappear upon the phase transition. To achieve the electric polarization reversal at 300 K, it is necessary to extend the metastable

FE3 region toward higher temperatures.

It should be mentioned here that in the previous study on BSCoFAO ceramics (polycrystals) by Hirose *et al.*[10], the magnetic-field reversal of P was indeed achieved at 300 K. This might be ascribed to a slight difference in chemical composition and/or sample form (single crystal vs. polycrystal). The metastability of the FE3 phase appears to be highly sensitive to local magnetic anisotropy, which may be governed by the Al concentration and/or grain boundaries.

D. Magnetic excitations in the ALC phase

As mentioned in the introduction, the Y-type hexaferrite BMFO is known to exhibit electromagnon excitation[15–17]. Thus, we expect that BSCoFAO also exhibits the electric-field-active magnon excitation, and that it would be applicable for magnetically-tunable light absorption devices working at room temperature. To observe the magnetic excitations in BSCoFAO, we performed inelastic neutron scattering measurements using the PTAX spectrometer.

Figure 9(a) shows unpolarized inelastic neutron scattering spectra of constant-Q scans on the $(0, 0, l)$ line at 4.5 K in zero field. We find a peak at around 7.5 meV at all measured l positions. We also performed constant-Q scans on the $(h, 0, 9 + q_{\rm IC})$ line, where $q_{\rm IC} = 0.75$, as show in Fig. 9(b). Although the peak becomes broader with increasing h, the spectral weight is shifted toward higher energies. These results are similar to the previous INS results on BMFO[16], which exhibits dispersion-less magnetic excitation along the c^* direction and a parabolic dispersion relation perpendicular to the c^* axis[16,17]. We also measured temperature dependence of the constant-Q profile at $(0, 0, 9 + q_{\rm IC})$, as shown in Fig. 9(c), revealing that the excitation energy is shifted toward lower values with increasing temperature.

To confirm that these inelastic signals are of magnetic origin, we performed IPNS measurements with p_N parallel to κ. In this configuration, magnon and phonon scatterings are observed only in the SF and NSF channels, respectively. Figure 9(e) shows the constant-Q profile at $(0, 0, 9 + q_{\rm IC})$. We found that the inelastic scattering signals at 7.5 meV come from the SF channel, confirming that this excitation is indeed of magnetic origin. This spectrum also shows that the diffusive scattering signals in the low-energy region are also magnetic in nature, although we could not identify the origin of the diffuse scattering at this moment.

To elucidate the microscopic picture of the magnetic excitaion at around 7.5 meV, we performed IPNS measurements at $(0, 0, 9+q_{\rm IC})$ and $(1, 0, 2.5)$ with p_N parallel to the x axis. Figure 9(f) shows the constant-Q profile at $(0, 0, 9 + q_{\rm IC})$, where NSF and SF scatterings correspond to the spin components oscillating along x and y directions, respectively. We observed the peak at around 7.5 meV in both the NSF and SF channels, indicating that magnetic moments are oscillating along both the x and y directions with the same amplitude. In the constant-Q profile at $(1, 0, 2.5)$, where $\boldsymbol{\kappa}$ is nearly parallel to the y axis (see Fig. 9(d)), we found that the inelastic scattering signals at around 7.5 meV arise mainly from the NSF scattering. This means that spin component oscillating along the z axis is absent. From these results, we conclude that the magnetic excitation at 7.5 meV is attributed to a phason-like mode, in which the magnetic moments are oscillating mainly in the plane perpendicular to the cone axis (c axis), as shown in Fig. 10(a).

In the previous study on BMFO[17], it was reported that the electromagnon excitation in the FE3 phase also has oscillating spin components perpendicular to the cone axis as shown in Fig. 10(b), and that the spin-wave mode can generate oscillating electric polarization along the c axis, $P_c(t)$, through the magnetostriction mechanism. Specifically, one may define local electric dipole moments (p_{local}) connecting neighboring L and S blocks as shown in Fig. 10(b). These local electric dipole moments are cancelled out in total in the static limit, because the crystal structure of BMFO has inversion symmetry. However, when the neighboring L (S) moments precess with a certain phase difference, the magnitudes of p_{local} can be slightly modified reflecting the exchange coupling $S_i^L(t) \cdot S_j^S(t)$. Taking into account the alternating arrangement of p_{local}, $P_c(t)$ is described as follows:

$$P_c(t) \propto \sum_i \{S_i^L(t) \cdot S_{i+1}^S(t) - S_{i+1}^S(t) \cdot S_{i+1}^L(t)\}. \tag{3}$$

By substituting the oscillating spin components observed in the IPNS measurements into Eq. (3), it was revealed that oscillating electric polarization can emerge when the neighboring L (S) moments oscillate with the phase difference of π[17].

We apply this magnetostriction mechanism to the ALC structure. On the basis of the phason-like spin-wave picture obtained from the IPNS measurements, the instantaneous deviations of the magnetic moments from their mean positions are schematically illustrated in Fig. 10(a). Note that we assumed that the deviations of the L and S moments are in opposite directions; if they were in the same direction, the spin-wave mode would cost no

exchange energy, and would be a Goldstone mode. Similarly to the case of the FE3 phase, macroscopic electric polarization can arise from the imperfect cancellation of p_{local} modified by the local exchange coupling. For instance, $S_1^L \cdot S_2^S$ and $S_2^S \cdot S_2^L$ are decreased and increased, respectively, by the deviations of the magnetic moments shown by the filled arrows in Fig. 10(a). Accordingly, this spin-wave mode can induce electric polarization along the c axis oscillating with the same frequency as that of the spin wave. To examine this scenario, a terahertz spectroscopy study on BSCoFAO is highly desired.

IV. SUMMARY

We investigated magnetic phase transitions in a multiferroic Y-type hexaferrite BSCoFAO by means of magnetization, electric polarization and neutron diffraction measurements using single-crystal samples. We revealed that BSCoFAO undergoes the magnetic phase transition from the proper-screw structure to the ALC structure at $T_1 = 360$ K in zero magnetic field, and that an application of $H_{\perp c}$ induces the FE3 phase, which has the double-fan structure with spin-driven ferroelectricity. The FE3 phase remains as a metastable state after removing magnetic field below ~ 250 K. This metastability is essential for the magnetic-field-reversal of the spin-driven electric polarization in this compound. We also performed the IPNS measurements in the ALC phase, revealing the magnetic excitation at around 7.5 meV, which is expected to be the electromagnon excitation. The IPNS measurements also revealed that the magnetic excitation is attributed to the spin components oscillating in the plane perpendicular to the cone axis. By comparing the present results with the previous IPNS study on BMFO[17], we suggest that the phason-like motions of the magnetic moments can induce oscillating electric polarization along the c axis via the magnetostriction mechanism.

Acknowledgements

The neutron scattering experiment at ORNL's HFIR was conducted along the proposal No. IPTS-13695.1, and was sponsored by the Scientific User Facilities Division, Office of Basic Energy Sciences, US Department of Energy. This study was supported in part by the U.S.-Japan Cooperative Program on Neutron Scattering. The images of the crystal and magnetic structures in this paper were depicted using the software VESTA[30] developed by

K. Momma.

---

* Electronic address: taro.nakajima@riken.jp

† Present address: Neutron Science and Technology Center, Comprehensive Research Organization for Science and Society (CROSS), Tokai, Ibaraki 319-1106, Japan

[1] T. Kimura, T. Goto, H. Shintani, K. Ishizaka, T. Arima, and Y. Tokura, Nature (London) **426**, 55 (2003).

[2] M. Kenzelmann, A. B. Harris, S. Jonas, C. Broholm, J. Schefer, S. B. Kim, C. L. Zhang, S.-W. Cheong, O. P. Vajk, and J. W. Lynn, Phys. Rev. Lett. **95**, 087206 (2005).

[3] T. Kimura, Annu. Rev. Condens. Matter Phys. **3**, 93 (2012).

[4] T. Kimura, G. Lawes, and A. P. Ramirez, Phys. Rev. Lett. **94**, 137201 (2005).

[5] S. Ishiwata, Y. Taguchi, H. Murakawa, Y. Onose, and Y. Tokura, Science **319**, 1643 (2008).

[6] K. Taniguchi, N. Abe, S. Ohtani, H. Umetsu, and T.-h. Arima, Appl. Phys. Express **1**, 031301 (2008).

[7] Y. S. Chai, S. H. Chun, S. Y. Haam, Y. S. Oh, I. Kim, and K. H. Kim, New Journal of Physics **11**, 073030 (2009).

[8] Y. Kitagawa, Y. Hiraoka, T. Honda, T. Ishikura, H. Nakamura, and T. Kimura, Nat. Mater. **9**, 797 (2010).

[9] S. H. Chun, Y. S. Chai, Y. S. Oh, D. Jaiswal-Nagar, S. Y. Haam, I. Kim, B. Lee, D. H. Nam, K.-T. Ko, J.-H. Park, et al., Phys. Rev. Lett. **104**, 037204 (2010).

[10] S. Hirose, K. Haruki, A. Ando, and T. Kimura, Appl. Phys. Lett. **104**, 022907 (2014).

[11] G. Wang, S. Cao, Y. Cao, S. Hu, X. Wang, Z. Feng, B. Kang, Y. Chai, J. Zhang, and W. Ren, J. Appl. Phys. **118**, 094102 (2015).

[12] H. Chang, H. B. Lee, Y.-S. Song, J.-H. Chung, S. A. Kim, I. H. Oh, M. Reehuis, and J. Schefer, Phys. Rev. B **85**, 064402 (2012).

[13] Y. S. Chai, S. Kwon, S. H. Chun, I. Kim, B. G. Jeon, K. H. Kim, and S. Lee, Nat. Commun. **5**, 4208 (2014).

[14] S. Hirose, S. Haruki, A. Ando, and T. Kimura, J. Am. Cer. Soc. **98**, 2104 (2015).

[15] N. Kida, S. Kumakura, S. Ishiwata, Y. Taguchi, and Y. Tokura, Phys. Rev. B **83**, 064422 (2011).

[16] N. Kida, D. Okuyama, S. Ishiwata, Y. Taguchi, R. Shimano, K. Iwasa, T. Arima, and Y. Tokura, Phys. Rev. B **80**, 220406 (2009).

[17] T. Nakajima, Y. Takahashi, S. Kibayashi, M. Matsuda, K. Kakurai, S. Ishiwata, Y. Taguchi, Y. Tokura, and T.-h. Arima, Phys. Rev. B **93**, 035119 (2016).

[18] N. Momozawa, Y. Yamaguchi, and M. Mita, J. Phys. Soc. Jpn. **55**, 1350 (1986).

[19] N. Momozawa, Y. Nagao, S. Utsumi, M. Abe, and Y. Yamaguchi, J. Phys. Soc. Jpn. **70**, 2724 (2001).

[20] S. Ishiwata, D. Okuyama, K. Kakurai, M. Nishi, Y. Taguchi, and Y. Tokura, Phys. Rev. B **81**, 174418 (2010).

[21] N. Momozawa and Y. Yamaguchi, J. Phys. Soc. Jpn. **62**, 1292 (1993).

[22] I. A. Sergienko and E. Dagotto, Phys. Rev. B **73**, 094434 (2006).

[23] H. Katsura, N. Nagaosa, and A. V. Balatsky, Phys. Rev. Lett. **95**, 057205 (2005).

[24] M. Mostovoy, Phys. Rev. Lett. **96**, 067601 (2006).

[25] H. B. Lee, Y.-S. Song, J.-H. Chung, S. H. Chun, Y. S. Chai, K. H. Kim, M. Reehuis, K. Prokeš, and S. Mat'aš, Phys. Rev. B **83**, 144425 (2011).

[26] H. B. Lee, S. H. Chun, K. W. Shin, B.-G. Jeon, Y. S. Chai, K. H. Kim, J. Schefer, H. Chang, S.-N. Yun, T.-Y. Joung, et al., Phys. Rev. B **86**, 094435 (2012).

[27] T. Ito, T. Ushiyama, Y. Yanagisawa, Y. Tomioka, I. Shindo, and A. Yanase, J. Cryst. Growth **363**, 264 (2013).

[28] As described in Sec. III B, this compound exhibits a noncollinear ferrimagnetic order under (relatively weak) magnetic field, which remains as a metastable state after removing magnetic field at low temperatures. We suggest that a very small faction of the ferrimagnetic order coexists with the ALC order in the PTAX experiment. The relatively low flipping ratio might be ascribed to existence of the randomly oriented ferrimagnetic domains.

[29] H. Sagayama, K. Taniguchi, N. Abe, T.-h. Arima, Y. Nishikawa, S.-i. Yano, Y. Kousaka, J. Akimitsu, M. Matsuura, and K. Hirota, Phys. Rev. B **80**, 180419 (2009).

[30] K. Momma and F. Izumi, J. Appl. Crystallogr. **41**, 653 (2008).

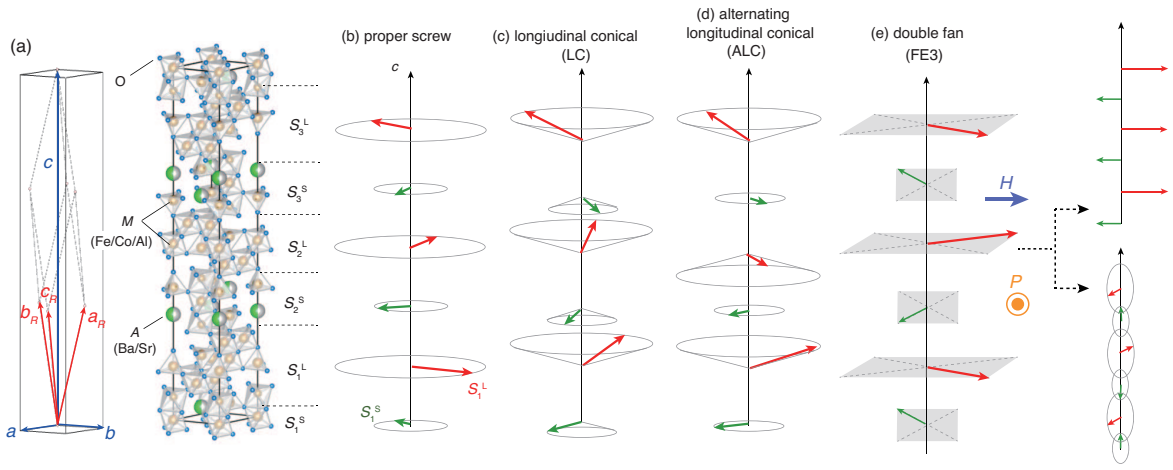

FIG. 1: (Color online) (a) The crystal structure of a Y-type hexaferrite with the hexagonal basis (a, b, c) and rhombohedral basis (a_R, b_R, c_R). For BSCoFAO, A sites are occupied by Ba or Sr. M sites mainly contain Fe, and are partly substituted by Co and Al. Schematic models of the (b) proper-screw, (c) LC (d) ALC, and (e) double-fan structures (and the staggered collinear and cycloidal components) on the basis of the block approximation.

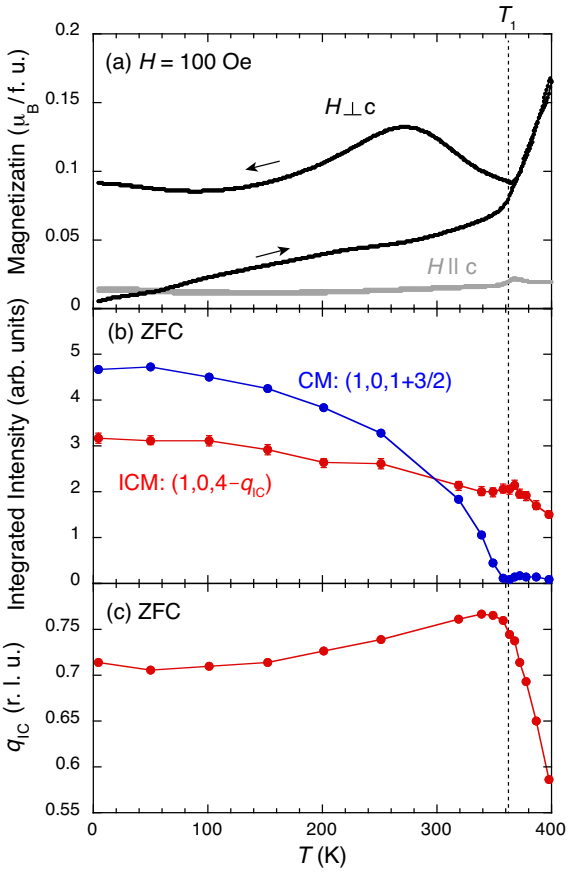

FIG. 2: (Color online) (a) Temperature dependence of magnetization under magnetic field of 100 Oe parallel and perpendicular to the c axis. The data for heating runs were measured after zero field cooling. [(b),(c)] Temperature dependence of (b) integrated intensities of the commensurate magnetic (CM) and incommensurate magnetic (ICM) reflections and (c) the wave vector of the incommensurate magnetic modulation $q_{\rm IC}$ on cooling.

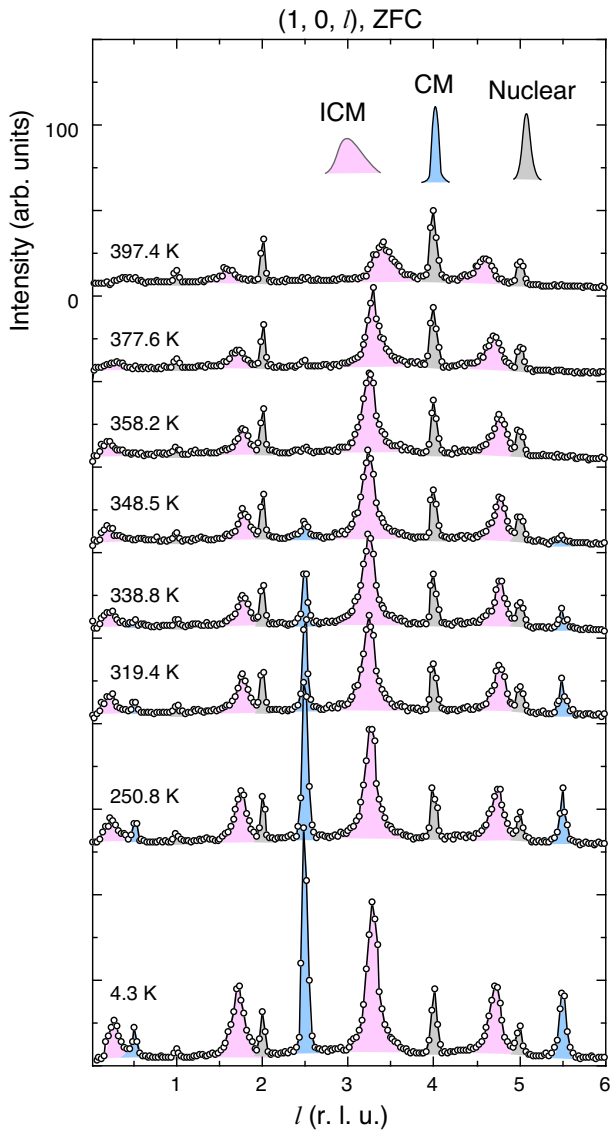

FIG. 3: (Color online) Temperature dependence of the unpolarized neutron diffraction profile on the $(1, 0, l)$ line measured on ZFC.

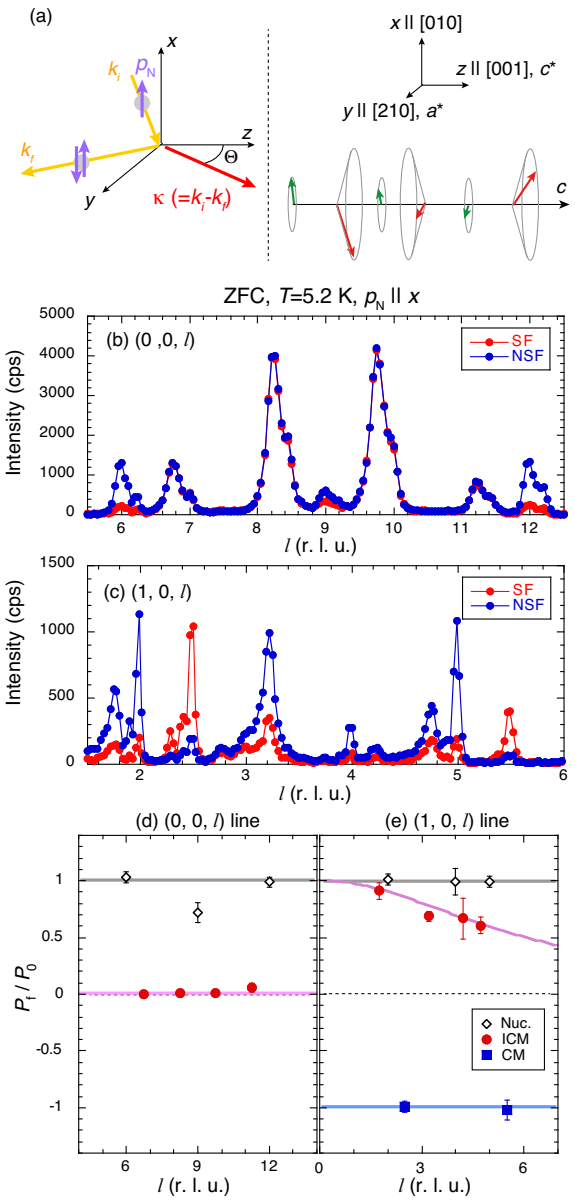

FIG. 4: (Color online) (a) Schematics showing relationships between the directions of κ, $p_{\rm N}$ and crystallographic axes and the Cartesian coordinate xyz. [(b),(c)] Polarized neutron diffraction profiles along the (b) $(0,0,l)$ and (c) $(1,0,l)$ lines measured with $p_{\rm N}$ parallel to the x axis at 5.2 K after ZFC. [(d),(e)] Observed and calculated l dependence of P_f/P_0 for (d) $(0,0,l)$ and $(1,0,l)$ lines.

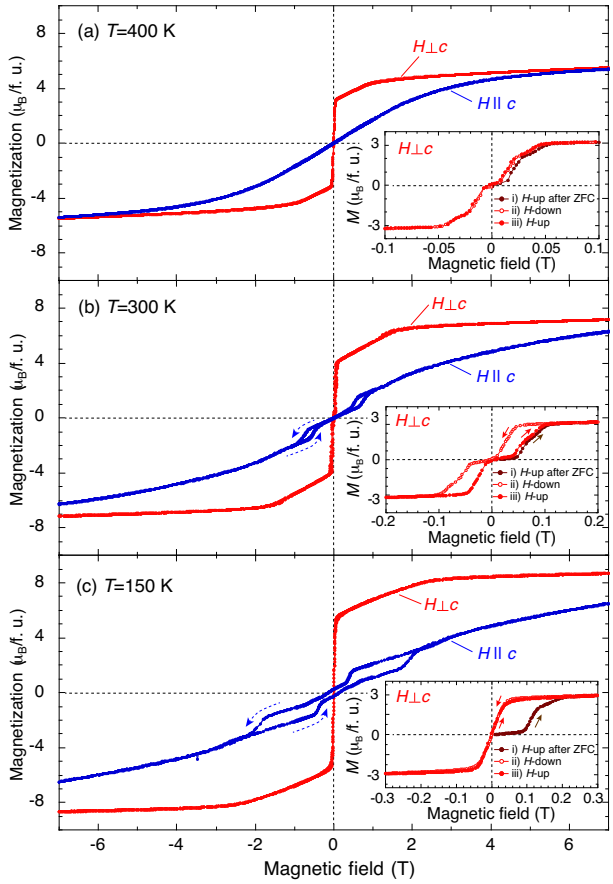

FIG. 5: (Color online) Magnetization curves measured under $H_{\|c}$ and $H_{\perp c}$ at (a) 400, (b) 300, and (c) 150 K. Insets show magnifications of low field regions of the M-$H_{\perp c}$ curves.

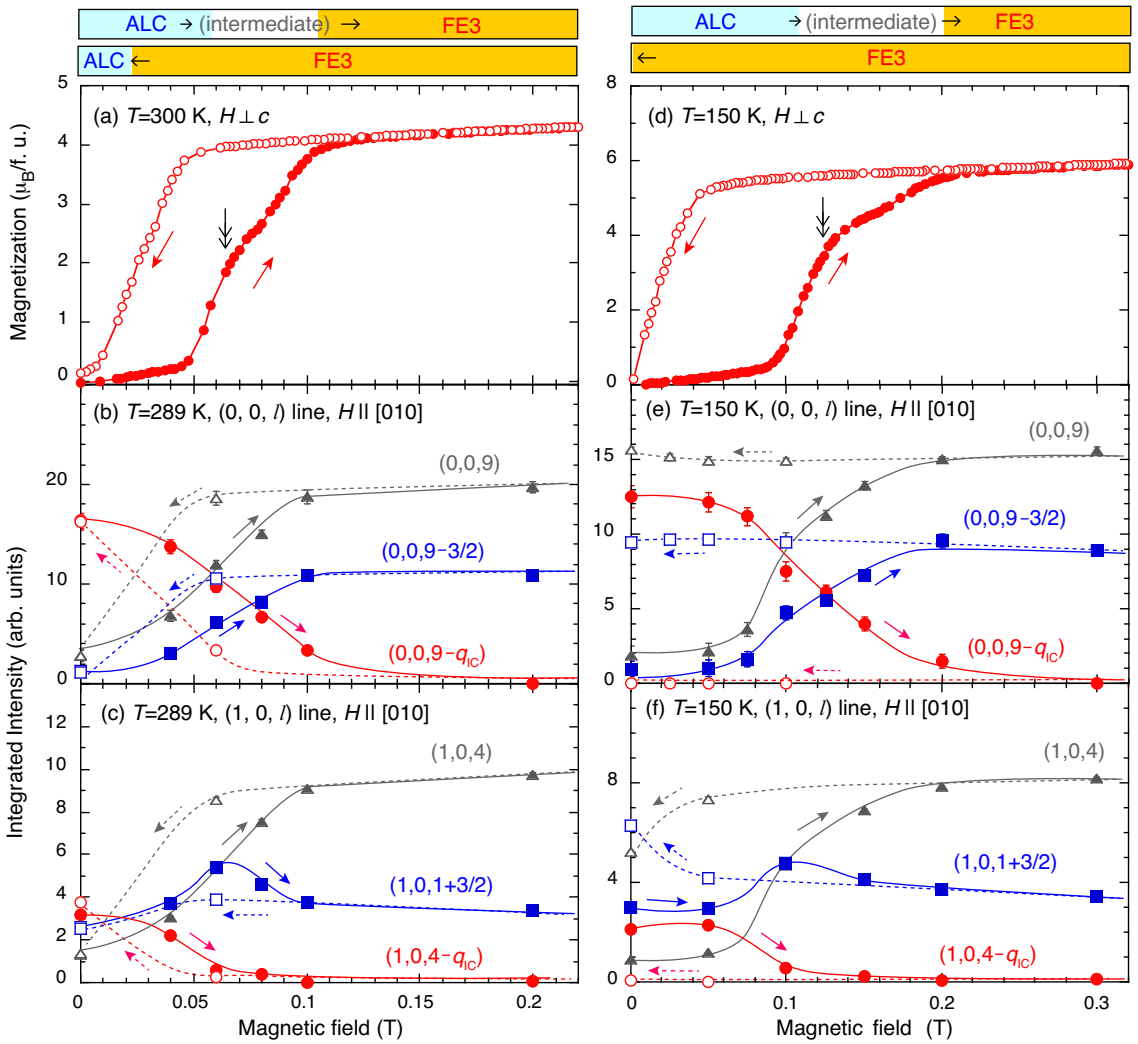

FIG. 6: (Color online) [(a),(d)] M-$H_{\perp c}$ curves measured after ZFC at (a) 300 and (d) 150 K. Doubled arrows indicate the inflection points, which may correspond to the transition to the intermediate phase (see text for details). Magnetic field dependence of integrated intensities of magnetic and nuclear reflections on the $(0, 0, l)$ line measured at (b) 289 and (e) 150 K, and those on the $(1, 0, l)$ lines measured at (c) 289 and (f) 150 K. The magnetic field was applied along the [010] direction. The sample was cooled in zero magnetic field before each measurement. Filled and open symbols denote the data points measured in field-increasing and decreasing processes, respectively. In (b), (c), (e), and (f), triangular, circular, and square symbols show the integrated intensities of nuclear, incommensurate magnetic, and commensurate magnetic reflections, respectively.

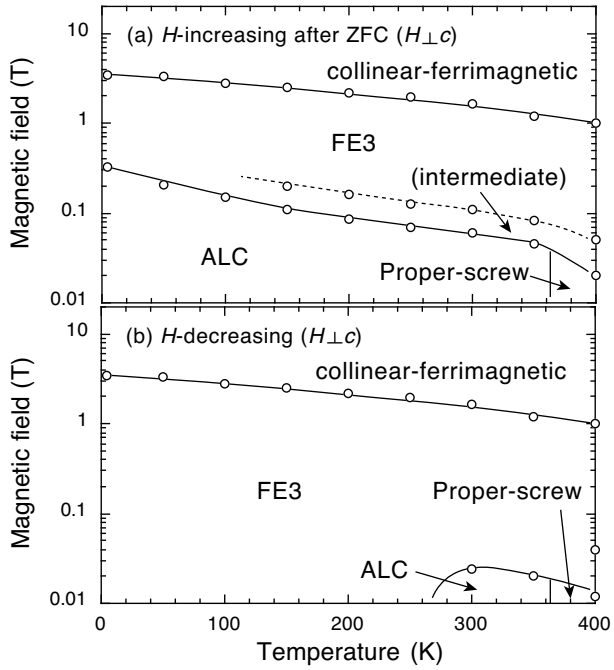

FIG. 7: $H_{\perp c}$-T magnetic phase diagram of BSCoFAO for (a) $H_{\perp c}$-increasing process after ZFC and (b) $H_{\perp c}$-decreasing process.

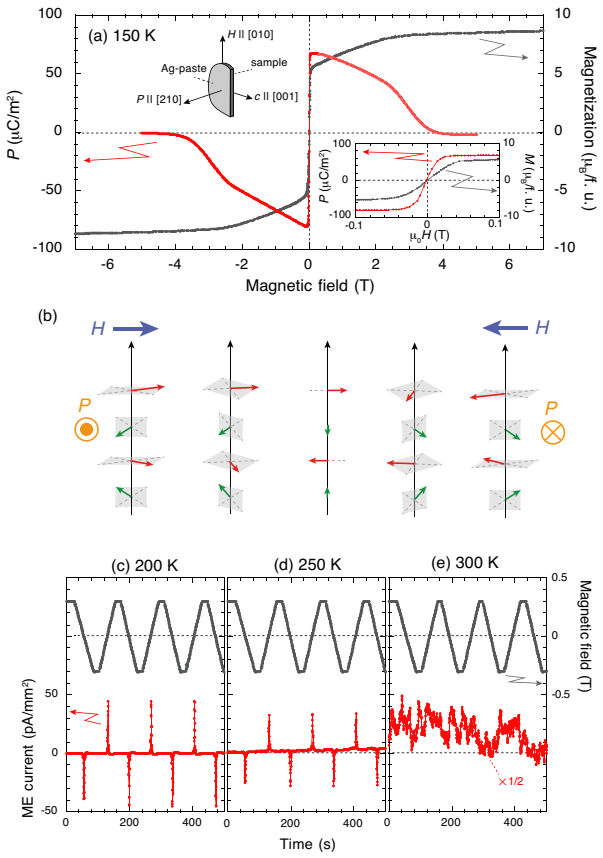

FIG. 8: (Color online) (a) Comparison of $H_{\perp c}$ dependence of P and magnetization at 150 K. Right-bottom and Left-top insets show a magnification of the low field region and a schematic showing the shape of the sample, orientation of the crystallographic axes and directions of magnetic field and electric polarization. (b) Schematic illustrations showing a possible spin arrangements during the magnetization reversal. [(c)-(e)] Displacement current (ME current) measured under sweeping magnetic field between ±0.3 T measured at (c) 200, (d) 250, and (e) 300 K.

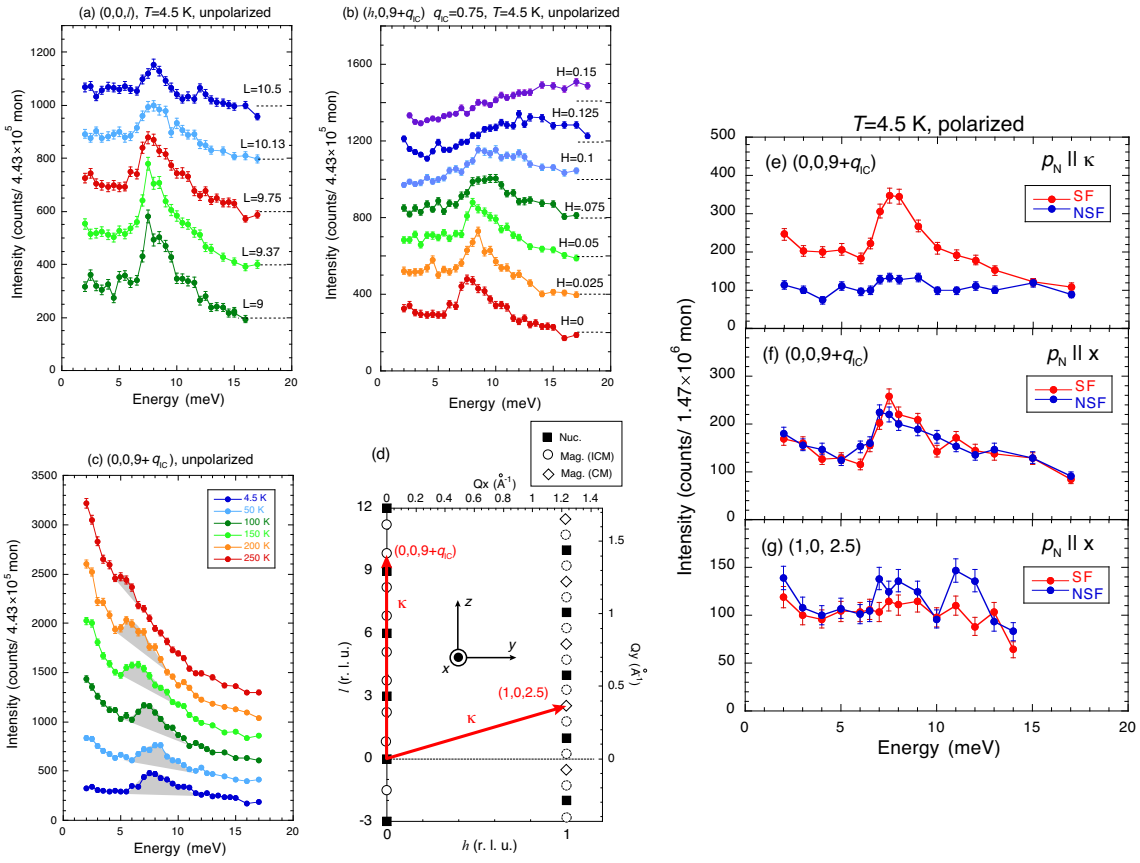

FIG. 9: (Color online) [(a),(b)] Unpolarized inelastic neutron scattering spectra measured by constant-Q scans on the (a) $(0, 0, l)$ and (b) $(h, 0, 9 + q_{\rm IC})$ lines, at $T = 4.5$ K after ZFC. (c) Temperature dependence of the unpolarized constant-Q profile at $(0, 0, 9 + q_{\rm IC})$. Note that the data are shifted by 200 for each, to enhance the visibility. The dashed lines are guides to the eyes. (d) A reciprocal lattice map of the $(h, 0, l)$ scattering plane. (e) IPNS spectrum measured by constant-Q scans with $p_{\rm N}$ parallel to κ at $(0, 0, 9 + q_{\rm IC})$ at 4.5 K after ZFC. [(f),(g)] IPNS spectra measured by constant-Q scans with $p_{\rm N}$ parallel to the x axis (perpendicular to the scattering plane) at (f) $(0, 0, 9 + q_{\rm IC})$ and (g) $(1, 0, 2.5)$ at 4.5 K after ZFC.

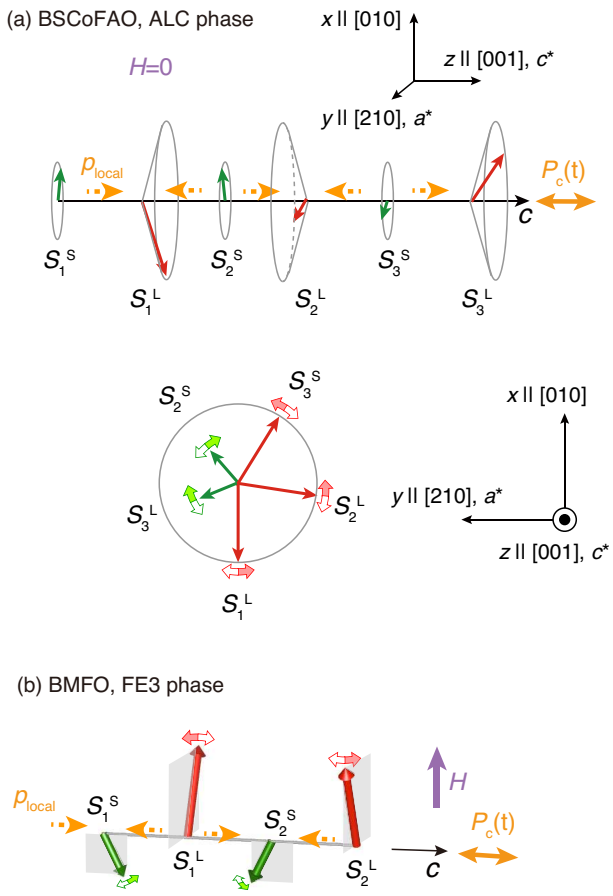

FIG. 10: (Color online) Schematic pictures of electromagnon modes in the (a) ALC phase in BSCoFAO and (b) FE3 phase of BMFO. Orange dotted arrows denote p_{local} embedded in the crystal structure. Pairs of filled and open arrows qualitatively show deviations of the magnetic moments from their mean position in the (possible) electromagnon modes.